Journal of Zhejiang University-SCIENCE A in press
www.jzus.zju.edu.cn; www.springer.com/journal/11582
E-mail: jzus_a@zju.edu.cn

Research Article
https://doi.org/10.1631/jzus.A2500552

Synergistic enhancement of machinability and surface integrity in bulk metallic glasses via cold plasma pretreatment and ultrasonic vibration-assisted micro-milling

Qilin LI[1,2*], Emek Babuskin KOCYIGIT[1,2*], Long YE[3], Nan YU[3], Pingfa FENG[1,2], Jianjian WANG[1,2]✉

[1]*State Key Laboratory of Tribology in Advanced Equipment, Department of Mechanical Engineering, Tsinghua University, Beijing 100084, China*
[2]*Beijing Key Laboratory of Precision/Ultra-precision Manufacturing Equipment and Control, Department of Mechanical Engineering, Tsinghua University, Beijing 100084, China*
[3]*Institute of Materials and Processes, School of Engineering, University of Edinburgh, Edinburgh, EH9 3FB, UK*

Abstract: Bulk Metallic Glasses (BMGs) exhibit exceptional properties, but are difficult to machine due to their high hardness and brittleness. In this study we propose a novel hybrid machining strategy integrating Cold Plasma (CP) pretreatment with Ultrasonic Vibration-assisted Micro-milling (UVAM), termed CP-UVAM, to overcome these challenges. We reveal the fundamental mechanism by which CP independently optimizes machining: it transforms the BMG surface from hydrophobic to super-hydrophilic (contact angle <10°) through oxidation and the introduction of polar groups, thereby enhancing lubricant penetration. Crucially, CP treatment increases the near-surface free volume, significantly improving plastic deformability, as evidenced by nanoindentation (15-20% reduction in first pop-in force) and nano-scratching tests. Four methods—Conventional Milling (CM), CP-assisted Milling (CPAM), UVAM, and CP-UVAM—were systematically compared. While CPAM alone delivered the best surface finish and least tool wear, UVAM achieved a 29.02% cutting force reduction at the cost of severe tool edge chipping. The synergistic CP-UVAM approach retained the force reduction advantage of UVAM (34.36% reduction vs CM) while dramatically mitigating UVAM-induced tool damage, reducing edge chipping by 43.97% and achieving superior surface consistency (an Sa value of 2.601 μm in the stable state). This study demonstrates that CP independently enhances BMG machinability and works synergistically with UVAM, enabling high-precision micro-milling of this challenging material through the combination of plasma-induced plasticity and wettability with ultrasonic vibration-assisted force reduction.

Key words: Bulk metallic glass; Micro-milling; Cold plasma; Ultrasonic vibration; Surface integrity

1 Introduction

Bulk Metallic Glasses (BMGs), which are characterized by an amorphous atomic structure, exhibit exceptional mechanical properties such as high strength and corrosion resistance. These attributes make them ideal for biomedical implants and microelectromechanical applications. However, their lack of grain boundaries also makes them difficult to machine, with conventional micro-milling causing rapid tool wear and surface defects (Chen et al., 2022). Thermal-based techniques like laser machining carry the risk of inducing crystallization above the glass transition temperature, while shear band formation during deformation generates microcracks that compromise surface integrity (Zhang and Huang, 2019).

Prior research has predominantly focused on optimizing conventional machining parameters to address these challenges. For instance, studies by Xie et al. (2017) emphasized the critical role of spindle speed and feed rate in preventing surface defects like melting and crystallization, which are detrimental to the amorphous structure. However, contrasting findings by Wang et al. (2020) suggested that spindle speed has a minimal impact on surface roughness (at

✉ Jianjian WANG, wangjjthu@tsinghua.edu.cn
* The two authors contributed equally to this work
Qilin LI, https://orcid.org/0009-0000-5318-5991
Jianjian WANG, https://orcid.org/0000-0001-8244-0760

Received Oct. 29, 2025; Revision accepted Jan. 4, 2026;
Crosschecked

least under their experimental conditions) – a discrepancy potentially caused by unexplored high-strain-rate machining regimes. Further investigations have elucidated the complex interplay of other parameters in this process. For example, Ray et al. (2019) demonstrated that the axial depth of cut significantly influences cutting forces, which increase with depth and decrease with higher spindle speeds; lower feed rates were interestingly found to increase forces, due to ploughing effects. Complementing this, Wang et al. (2020) highlighted the significant role of the feed ratio, identifying a critical value for pronounced size effects, and also found that burr size is more sensitive to feed rate and axial depth than to spindle speed.

The aforementioned work highlights the intricate balance required in parameter selection for BMG machining in order to manage forces, surface quality, and defects. However, these studies collectively reveal a fundamental limitation: optimization within the framework of conventional micro-milling (CM) is inherently constrained by the material's intrinsic brittleness and thermal sensitivity (Chen et al., 2022). Adjusting process parameters alone is often insufficient to overcome these inherent property barriers, indicating a pressing need for innovative machining strategies that can actively alter the machining interface or the material's local properties, so as to enable high-quality processing with low damage.

Cold plasma-assisted machining (CPAM) presents a complementary strategy by directly modifying the BMG's near-surface properties. In applications of this technology, Liu et al. (2021) and Mustafa et al. (2019) demonstrated plasma's effectiveness in machining titanium and Inconel alloys. Later, a pivotal study by Wang et al. (2024) on atmospheric pressure cold plasma jet (APCPJ) assisted micro-milling of BMGs confirmed that APCPJ pretreatment could markedly improve machinability, specifically achieving reductions in surface roughness (up to 38.2%) and cutting forces (up to 30.9%). This improvement was attributed to a plasma-induced increase in near-surface free volume, which promotes the formation of multiple shear bands and thereby improves ductility (Lv et al., 2022).

Despite these promising results, this foundational research was conducted under dry machining conditions, which inherently limit the scope of application. It focused exclusively on the mechanical and microstructural modifications induced by plasma, leaving a key physicochemical effect unexplored: the plasma-mediated transformation of the BMG surface from hydrophobic to hydrophilic. This change in wettability – which could drastically improve the penetration and efficacy of coolants and lubricants – represents an untapped avenue for process enhancement. Exploiting this effect is particularly crucial for limiting heat accumulation and the risk of temperature-induced crystallization at high material removal rates (Bakkal et al., 2004), but these challenges are not addressable in a dry machining context.

Moreover, despite the advancements in CPAM and the separate progress in UVAM, no prior study has systematically investigated the synergistic effects of combining cold plasma pretreatment with ultrasonic vibration for BMG machining. The combined potential of plasma-enhanced surface modification and UVAM's intermittent cutting mechanism remains unexplored, particularly in addressing BMGs' dual challenges of brittleness and thermal sensitivity. This study bridges this gap by pioneering an integrated approach, examining how plasma treatment can augment UVAM by improving lubricant penetration, reducing cutting forces, and suppressing shear band formation, while also mitigating heat-induced crystallization. Our work aims to establish a hybrid machining strategy that unlocks higher precision and efficiency for BMG micro-milling applications.

2 Materials and methods

2.1 Materials

The experiments utilized Vitreloy 1 (Zr41.2Ti13.8Cu12.5Ni10Be22.5 at%), a benchmark Zr-based BMG selected for its exceptional properties. The Vitreloy 1 samples (25 mm × 25 mm × 2 mm) were polished to ensure measurement consistency, as shown in Fig. 1a. To eliminate surface effects in the water contact angle measurements, nano-indentation, and nano-scratching tests, all samples underwent standardized preparation of ultrasonic cleaning in ethanol followed by complete drying.

2.2 Experimental protocol

We employed a systematic experimental approach to evaluate the effects of cold plasma treatment (**Fig. 1**b) and micro-milling (**Fig. 1**c) on BMGs. The treatment of BMGs was performed using a state-of-the-art plasma processor from Zhenhua Plasma. To ensure that the plasma was uniformly distributed across the surface of the BMGs, a motion table system (depicted in **Fig. 1**d) was used to facilitate the movement of the BMG samples beneath the plasma jet, enhancing the consistency and quality of the plasma treatment. The parameters of the plasma treatment for the BMG samples are listed in **Table 1**.

Table 1 Plasma treatment parameters

Parameter	Specification
Working gas	Compressed Air
Gas pressure	0.4 MPa
Operating temperature	~50 °C
Nozzle diameter	2 mm
AC power frequency	18~25 kHz
Total treatment time	50/100/150/200 s

The investigation began with comprehensive material characterization, where water contact angle measurements (KINO SL250) were made to quantify the plasma-induced surface wettability changes, nanoindentation and nano-scratching tests (Anton Paar NHT2) assessed mechanical property changes, including Young's modulus; moreover, plasticity characteristics were determined through analysis of pop-in events and friction coefficients. To ensure the reliability of the nano-scratching results, each test was repeated three times (designated as Scratch Test #1, #2, and #3) under identical conditions. This repetition enabled verification of the consistency of the measured parameters, and included the analysis of pop-in events and friction coefficients. The reported data for Young's modulus and plasticity are derived from this statistically validated set of repeated measurements.

Building upon these material property evaluations, the machining performance was examined across four distinct micro-milling approaches: conventional milling (CM), cold plasma-assisted milling (CPAM), ultrasonic vibration-assisted milling (UVAM), and cold plasma combined with ultrasonic vibration-assisted milling (CP-UVAM). The milling parameters are listed in **Table 2**. The micro-milling tool had a nominal diameter of 1 mm and was made of cemented carbide with a diamond-like coating. The tool parameters are listed in **Table 3.** To ensure the reliability of the performance evaluation, three consecutive grooves (designated as Groove #1, #2, and #3) were machined under each experimental condition. This design served two purposes: first, to verify the repeatability of the results by providing multiple datasets for each key metric, and second, to accumulate sufficient cutting length to induce a consistent and comparable level of tool wear for observation and analysis. Each method's effectiveness was then evaluated using three key metrics: the surface quality was analyzed by confocal laser microscopy (Zeiss LSM900), the cutting forces were measured with a dynamometer (Kistler 9256), and the tool wear was assessed via optical microscopy (HIROX HR-2500). Data and observations from all three grooves were utilized in this assessment.

Table 2 Milling parameters used in the experiments

Parameter	Specification
Spindle speed (rpm)	22,000
Feed rate (mm/min)	30
Depth of cut (μm)	10
Frequency (kHz)	19.89

Table 3 Milling tool parameters

Parameter	Specification
Nominal diameter (mm)	1
Number of flutes	2
Helix angle (°)	30
Shaft width (mm)	4
Shaft length (mm)	50
Material base	Cemented carbide
Coating	Diamond-like coating
Hardness (HV)	>7000
Temperature resistance (°C)	Up to 500°C
Nominal diameter (mm)	1

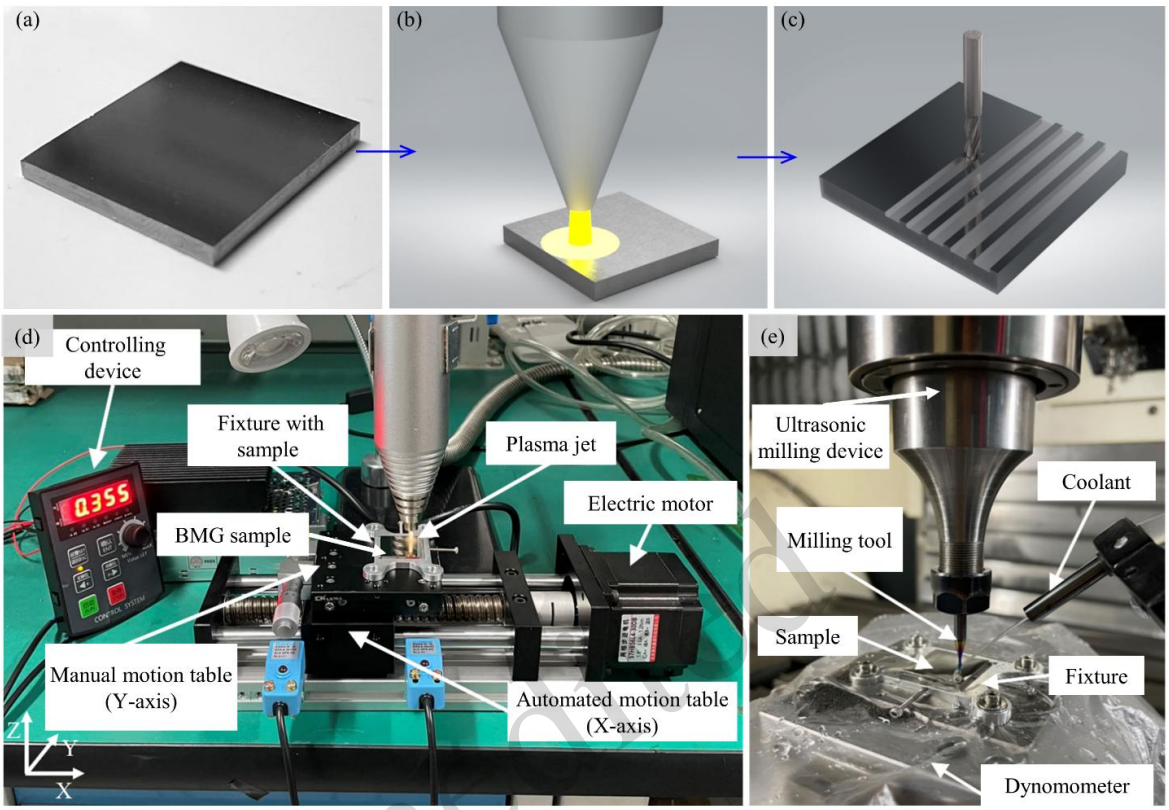

Fig. 1 BMG sample and the experimental process. (a) Polished sample; (b) Schematic diagram of plasma treatment; (c) Schematic diagram of the micro-milling process; (d) Experimental setup of plasma treatment for a BMG sample; (e) Experimental setup of the micro-milling process for a BMG sample

3 Results and discussion

3.1 Surface wettability

The investigation into the effects of cold plasma treatment on the surface wettability of BMG was conducted by measuring contact angles across a range of treatment times: 0 seconds (i.e. untreated), 50 seconds, 100 seconds, 150 seconds, and 200 seconds. The contact angles were quantified at six distinct points per treatment duration to ensure comprehensive coverage and accuracy of the data. The results of these investigations are presented in **Fig. 2**a.

The untreated BMG samples exhibited an average contact angle of 65.582° with a narrow standard deviation (SD: 2.859), reflecting uniform hydrophobic properties. The 50-second plasma treatment drastically reduced the angle to 27.574° (SD: 2.902), confirming the rapid enhancement of surface hydrophilicity. Extending the treatment to 100 and 150 seconds further lowered the angles to 24.296° (SD: 3.237) and 17.848° (SD: 3.348), respectively, although the increased deviations suggested slight inhomogeneity in the effect of the plasma. At 200 seconds, all contact angles were under 10°, indicating a transition to super-hydrophilicity; this is likely due to extensive surface oxidation or topographic changes induced by prolonged plasma exposure.

These results demonstrate that cold plasma treatment effectively modulates BMG wettability, with longer durations yielding progressively more hydrophilic surfaces. At the 200 second mark, the contact angles on all measured points were 0 degrees, indicating that the values fell below the measurable threshold of the contact angle measurement system (which cannot measure angles under 10 degrees). The mechanism by which plasma treatment reduces the wettability (or enhances the hydrophilicity) of Zr-based BMG surfaces primarily involves plasma-induced oxidation and surface functionalization, as shown in Fig. 2b. Reactive oxygen species (O·) generated in the plasma interact

with the Zr-rich surface, forming a hydrophilic oxide layer (e.g., ZrO_2) and introducing polar functional groups (e.g., –OH) through oxidation and hydrolysis (Yamamura et al., 2010). Simultaneously, plasma etching removes organic contaminants and creates nanoscale roughness, amplifying wettability via the Wenzel effect. Prolonged treatment (e.g., 200 seconds) leads to complete surface coverage by hydrophilic groups and optimal topography, driving the contact angle to under 10° (superhydrophobicity); the synergy between chemical modification and physical roughening enables this transition. These findings underscore the impact of plasma treatment duration on BMG surface wettability. Therefore, subsequent plasma-treated specimens were all pre-treated for 200 seconds to ensure consistent surface wettability.

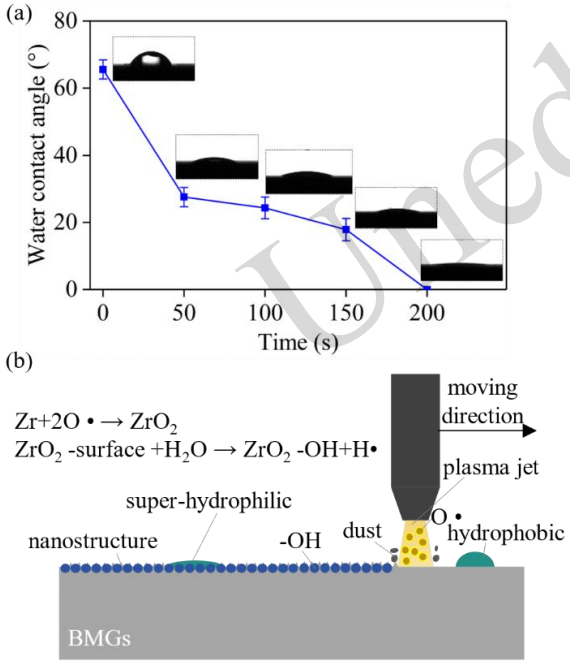

Fig. 2 Surface wettability of BMG by cold plasma treatment. (a) Water contact angle of a BMG sample. (b) The mechanism of transition from hydrophobic to super-hydrophilic.

3.2 Mechanical properties

Nanoindentation tests were conducted to compare the Young's modulus and pop-in phenomena between untreated BMG and BMG treated with plasma for 200 seconds. These tests were carried out at maximum loads of 20 mN and 50 mN. The summarized results for a maximum load of 20 mN are displayed in **Fig. 3**a, while those for a maximum load of 50 mN are presented in **Fig. 3**b.

Under a load of 20 mN, the average Young's modulus for the untreated BMG samples was 126.382 GPa, with a standard deviation of 721 MPa, reflecting a high degree of material stiffness and elasticity. For the cold plasma-treated BMG, the average modulus decreased slightly to 124.476 GPa, and had increased variability (standard deviation of 913 MPa). This minor reduction suggests a slight alteration in the elastic properties due to plasma treatment. Under a load of 50 mN, the Young's modulus for the untreated BMG samples averaged 128.545 GPa with a significant standard deviation of 1795 MPa, suggesting considerable variability in material responses. For the plasma-treated samples, the modulus decreased slightly to 126.944 GPa, with a reduced standard deviation of 1150 MPa. This reduction in the modulus and its variability compared to untreated samples suggests a subtle softening of the material, which aligns with the trend of observations at 20 mN.

The most notable difference lies in the first pop-in phenomenon. Under a maximum load of 20 mN, the average force required to initiate the first pop-in event decreased from 8.80 ± 1.8 mN in untreated samples, to 7.51 ± 0.9 mN in plasma-treated samples. This reduction in pop-in initiation force indicates a lower critical stress for initial plasticity, likely due to plasma-induced surface modifications (e.g., a reduced energy barrier for shear transformation zone activation (Liu et al., 2023)). A similar trend was observed under 50 mN loading, where the pop-in force dropped from 25.67 ± 3.4 mN (untreated) to 20.53 ± 1.7 mN (treated), representing a more significant reduction (~20%) compared to the 20 mN case (~15%). These results imply that plasma treatment facilitates earlier yielding during indentation, which may have critical implications for micro-milling processes where controlled initiation of plasticity is required.

In the deformation of BMGs, pop-in events in the force-displacement curves are associated with the nucleation and propagation of shear bands (Schuh and Nieh, 2003). The overall deformation behavior of BMGs is characterized by displacement bursts (plastic steps), which correspond to sudden shear band activity, separated by elastic deformation

regimes (Puthucode et al., 2008). The force at which the first pop-in occurs marks the onset of shear band nucleation (rather than dislocation nucleation, since BMGs lack crystalline defects). The lower pop-in initiation force observed in cold plasma-treated BMGs suggests that the treatment facilitates shear band formation, thereby enhancing the plastic deformability.

In addition to nano-indentation tests, nano-scratching tests were conducted in order to examine the progression of the tangential force F_t in response to a linearly increasing normal force F_n applied over a scratch length of 500 μm. To eliminate external influences, this experiment was repeated three times. The results are displayed in **Fig. 3**c-d, where **Fig. 3**c presents the tangential force trajectories for untreated BMGs, and **Fig. 3**d presents the tangential force trajectories for BMGs with plasma treatment.

The tangential force profiles are strongly influenced by the pop-in phenomenon, which is even more pronounced in this case due to prominent force spikes. Notably, cold plasma treatment significantly alters the response of the BMG samples. The tangential force curves for the plasma-treated BMGs exhibit markedly greater stability than those of the untreated samples. In the untreated BMGs (**Fig. 3**c), the force profiles display substantial irregularities, featuring abrupt jumps or spikes. These spikes, which are linked to the pop-in phenomenon, reflect discrete shear band nucleation; this is consistent with observations from nanoindentation tests. Their presence suggests sudden rises in frictional resistance due to shear band initiation during scratching. Moreover, the erratic force fluctuations indicate non-uniform deformation behavior and poor mechanical stability. In contrast, the plasma-treated BMGs (**Fig. 3**d) demonstrate significantly smoother force progression with fewer and less pronounced spikes. This improvement implies that plasma treatment effectively modifies the BMG surface or near-surface microstructure, yielding a more stable and consistent scratch response. The reduced number of pop-in events and smoother frictional profiles further suggest that plasma treatment enhances the plastic deformability of BMGs, likely by improving ductility or suppressing brittleness. As such, this enables better accommodation of scratching-induced stresses.

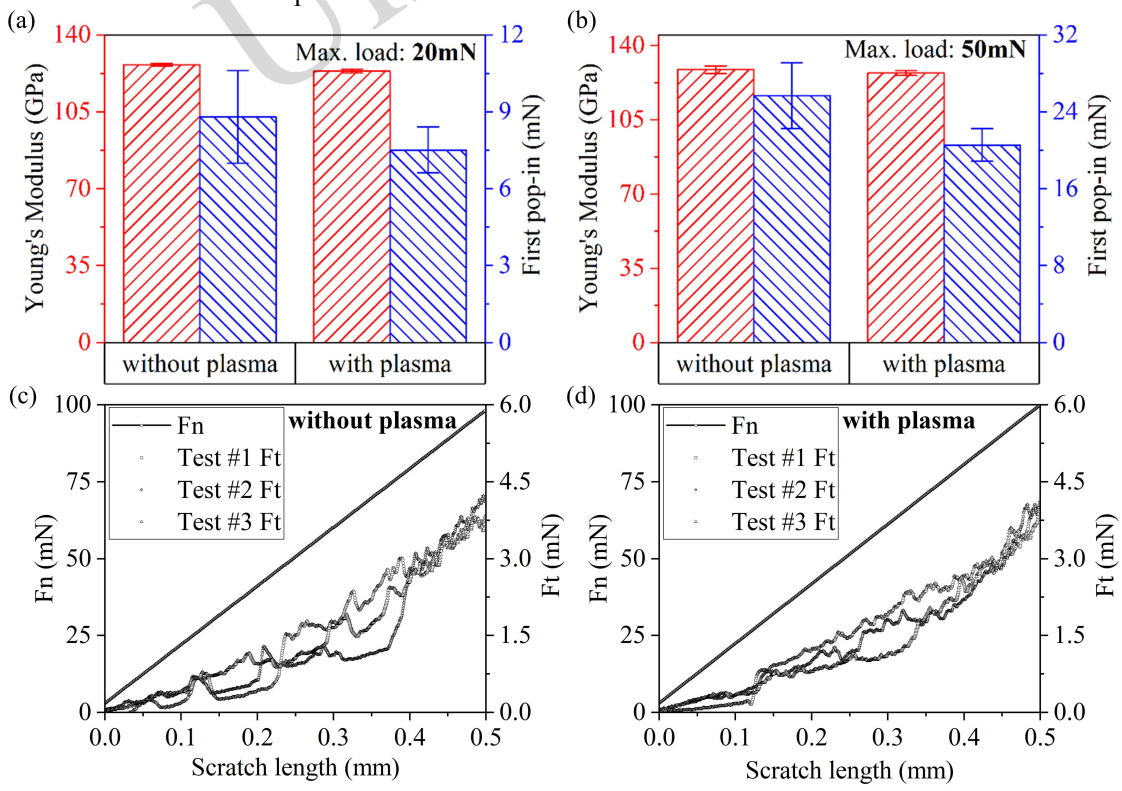

Fig. 3 Nano-indentation and nano-scratch results of BMG samples. (a) Young's modulus and first pop-in phenomena

under a maximum load of 20 mN. (b) Young's modulus and first pop-in phenomena under a maximum load of 50 mN. (c) Nano-scratch results for BMGs without plasma treatment. (d) Nano-scratch results for BMGs with plasma treatment

3.3 Micro-milling performance

3.3.1 Milling force

The results of the investigation of cutting forces during the micro-milling of BMGs using various assisted milling approaches are shown in **Fig. 4**a. The analysis of CM revealed a clear trend of increasing cutting forces across the three grooves (#1/#2/#3). The initial forces were relatively low but rose significantly by the third groove, predominantly due to tool wear and the inherent material properties of BMGs, such as high hardness and limited plastic deformability. Sudden spikes in cutting forces – particularly in groove #2 – indicated areas of substantial tool wear. This led to a stable state in groove #3 with a high total average cutting force of 861 mN, reflecting the variability and challenge of maintaining consistent cutting conditions.

CPAM initially exhibited behavior similar to CM, with an average cutting force of 321 mN at the beginning of groove #1. An initial spike in groove #1 resulted in a comparatively high total average cutting force of 413 mN for this groove. However, from groove #2 onwards, the forces stabilized significantly, suggesting improved control over tool wear and process stability due to the cold plasma treatment. By the stable state in groove #3, the total average cutting force was reduced to 681 mN, representing a significant reduction of 20.90% compared to CM. This observation aligns with the findings of Wang et al. (2024), who reported a 23.3–30.9% decrease in cutting forces during cold plasma-assisted micro-milling of BMGs under dry conditions. The consistency in the direction and magnitude of force reduction supports the established mechanism wherein plasma-induced increases in near-surface free volume enhance the plastic deformability, thereby reducing the specific cutting energy. Additionally, the total standard deviation at the stable state within groove #3 decreased by 31.90% to 49 mN. Furthermore, the standard deviation between the three grooves decreased by 48.84%, from 293 mN to 150 mN, indicating enhanced stability and reduced variability.

UVAM demonstrated a substantial reduction in initial cutting force in groove #1 to 168 mN, representing a 39.79% and 47.66% decrease compared to CM and CPAM, respectively. However, this reduction was not sustained beyond groove #1, with noticeable increases in cutting forces and standard deviations occurring from groove #2 onwards, due to significant tool wear. By groove #3, the process reached a stable state with a total average cutting force of 611 mN – a 29.02% reduction compared to CM. This level of force reduction is in accordance with the range (up to 30%) reported for UVAM of various difficult-to-cut materials, including BMGs, as documented by Gao et al. (2023) and Shan et al. (2020). The primary mechanism—intermittent cutting leading to lower average forces—is thus validated for BMG micro-milling. However, the concurrent rise in force variability and standard deviation observed in our results points to an accelerated and unstable tool wear process under UVAM. This is a specific challenge that is not often highlighted in force-focused literature, but is nonetheless crucial for process reliability (Chen et al., 2022). Despite the improved average forces, UVAM exhibited a major issue with increased total standard deviation within the grooves themselves, resulting in a 65.16% rise from 73 mN to 120 mN as compared to CM in groove #3.

CP-UVAM demonstrated the most promising results, characterized by an almost linear increase in the total average cutting force in groove #1 to approximately 500 mN, without any sudden bursts. This resulted in the highest total average cutting force in groove #1, but also facilitated a quick transition to a stable state. Despite the initially high forces, CP-UVAM held the force level from groove #1 nearly constant and achieved the lowest stable-state average cutting force in groove #3 at 565 mN, representing a 34.36% reduction compared to CM. This synergistic force reduction exceeds the individual contributions of CPAM (20.90%) and UVAM (29.02%), suggesting a non-additive enhancement effect. While direct comparisons are scarce due to the novelty of this hybrid approach, such a result logically integrates the known benefits: the plasma-induced surface plasticity likely lowers the specific cutting resistance, upon which the intermittent action of UVAM operates more

effectively, leading to greater net force reduction. This means that CP-UVAM also exhibited the most substantial reduction in the standard deviation between grooves, with a 90.22% decrease to 29 mN compared to CM. Additionally, the combination of CP and UVAM effectively mitigated the increased total standard deviation observed in UVAM within groove #3, reducing the increase compared to CM from 65.16% to 6.97%.

To conclude, CPAM and UVAM each succeeded in reducing the average cutting forces at the stable state compared to CM by 20.90% and 29.02%, respectively. Such findings are consistent with and extend the respective bodies of literature for these individual techniques (Gao et al., 2023). CPAM additionally enhanced the process stability by reducing the standard deviation between grooves by 48.84% and the standard deviation at the stable state by 31.90%. Overall, in terms of exerted cutting forces, the combined approach of CP-UVAM emerged as the most effective for micro-milling BMGs, with a decrease in average cutting forces at the stable state of 34.36% compared to CM. This method further reduced the cutting forces achieved by CPAM and UVAM individually, and also through synergistic effects suppressed the decrease in process stability observed with UVAM, achieving a reduction in the standard deviation between grooves by 90.22% compared to CM. The superior and stable force performance of CP-UVAM underscores the value of our hybrid strategy, as it effectively combines the force-reduction merits of both techniques while counteracting the key limitation of standalone UVAM – increased instability.

3.3.2 Surface quality

The findings on surface roughness are graphically depicted in **Fig. 4**b. Conventional micro-milling of BMGs showed a clear progression of surface degradation across the grooves; the surface roughness measurements revealed a consistent increase in roughness from groove #1 to groove #3. The average surface roughness increased from 1.273 μm to 1.863 μm, with the standard deviation between the grooves being 0.311 μm. This significant increase in surface roughness indicates severe tool wear, leading to substantial degradation of surface integrity. This trend of deteriorating surface quality with progressive tool wear in conventional BMG machining is consistent with observations in prior studies, which have attributed it to BMG's low fracture toughness and tendency for brittle fracture, thus leading to unstable chip formation and surface damage.

CPAM demonstrated a more stable and consistent surface quality compared to CM. Despite a higher initial surface roughness in groove #1 (1.629 μm), the consistency in surface quality was higher, with minimal increases in roughness and lower standard deviations across the grooves. The average surface roughness increased only slightly to 1.701 μm in groove #2, and remained steady at 1.698 μm in groove #3. The standard deviation between the grooves was 0.040 μm, indicating a more uniform and stable milling process. This is further evidenced by the fact that the surface roughness at the stable state was reduced by 8.87% compared to CM. The observed improvement in surface finish and, more notably, the dramatic enhancement in process stability (evidenced by reduced standard deviations) align with and extend the findings of Wang et al. (2024); they reported roughness reductions of 37.7–38.2% in dry CP-assisted milling of BMGs. While the percentage reduction is more modest in our lubricated study, the critical improvement is in consistency. This supports the proposed mechanism whereby a plasma-induced free volume increase promotes more stable plastic deformation and mitigates brittle fracture, leading to a more predictable and uniform surface generation. Moreover, the standard deviation at the stable state and the standard deviation between the grooves were reduced by 53.01% and 87.01%, respectively. These improvements can likely be attributed to the enhanced plastic deformability of the material following cold plasma treatment, which contributed to reduced tool wear and, consequently, a well-maintained surface quality.

UVAM exhibited a substantial increase in surface roughness and defects after groove #1, leading to significant surface degradation; the average surface roughness increased from 2.273 μm in groove #1 to 2.854 μm in groove #3. The standard deviation between the grooves was 0.301 μm, reflecting high variability and significant tool wear. The additional impact generated by ultrasonic vibrations created high stress on the tool and surface, exacerbating the

wear and leading to pronounced surface defects. This finding presents a nuanced perspective compared to some literature which has primarily highlighted UVAM's benefits for force reduction and surface finish in other materials (Li et al., 2025). Our results for BMGs indicate that vibrational energy – while reducing average forces – can accelerate tool degradation in this hard, brittle material, which in turn severely compromises surface quality. This aligns with the caution raised by Chen et al. (2022) regarding surface deterioration and tool damage in UVAM of BMGs when parameters exceed an optimal window, underscoring the material-specific challenges of applying UVAM to BMGs.

CP-UVAM showed far more promising results. The influence of cold plasma on this approach was similar to the improvements observed when comparing CPAM to CM. The topographies indicated minimal pitting and surface defects, with a relatively uniform texture throughout all the grooves. This is also quantitatively reflected in the development of the surface roughness measurements. The average surface roughness for groove #1 was 2.405 μm, increasing slightly to 2.507 μm in groove #2 and 2.601 μm in groove #3. The standard deviation between the grooves was 0.098 μm, which is 67.48% smaller than that of UVAM; this demonstrates a decisive synergistic effect. While standalone UVAM degraded the surface quality, including CP pretreatment effectively counteracted this effect. The plasma-induced surface plasticity and improved lubricant wettability likely mitigated the abrasive and impact-related wear mechanisms exacerbated by vibrations, leading to more stable tool conditions and consequently a more consistent surface. This synergy in achieving stable surface generation is a novel finding, as no prior study has investigated the combined approach of CP-UVAM for BMGs. Additionally, the standard deviation in the stable state was reduced by 17.01%, and the surface roughness in the stable state decreased by 8.85%.

Overall, the pre-treatment of BMGs with cold plasma resulted in significant improvements in surface quality and process stability. CPAM led to more stable and consistent surface quality compared to CM. This same trend was observed when comparing CP-UVAM with UVAM, confirming the previous investigations of enhanced surface wettability and plastic deformability resulting from cold plasma treatment. These findings collectively affirm that plasma modification addresses core instability issues in BMG machining. The stark contrast between the degrading surfaces in UVAM and the stabilized surfaces in CP-UVAM powerfully illustrates that the benefits of vibration-assisted machining for BMGs are fully realizable only when coupled with a surface-conditioning strategy like cold plasma treatment to manage tool-material interactions. This conclusion is also reflected in the cutting force results.

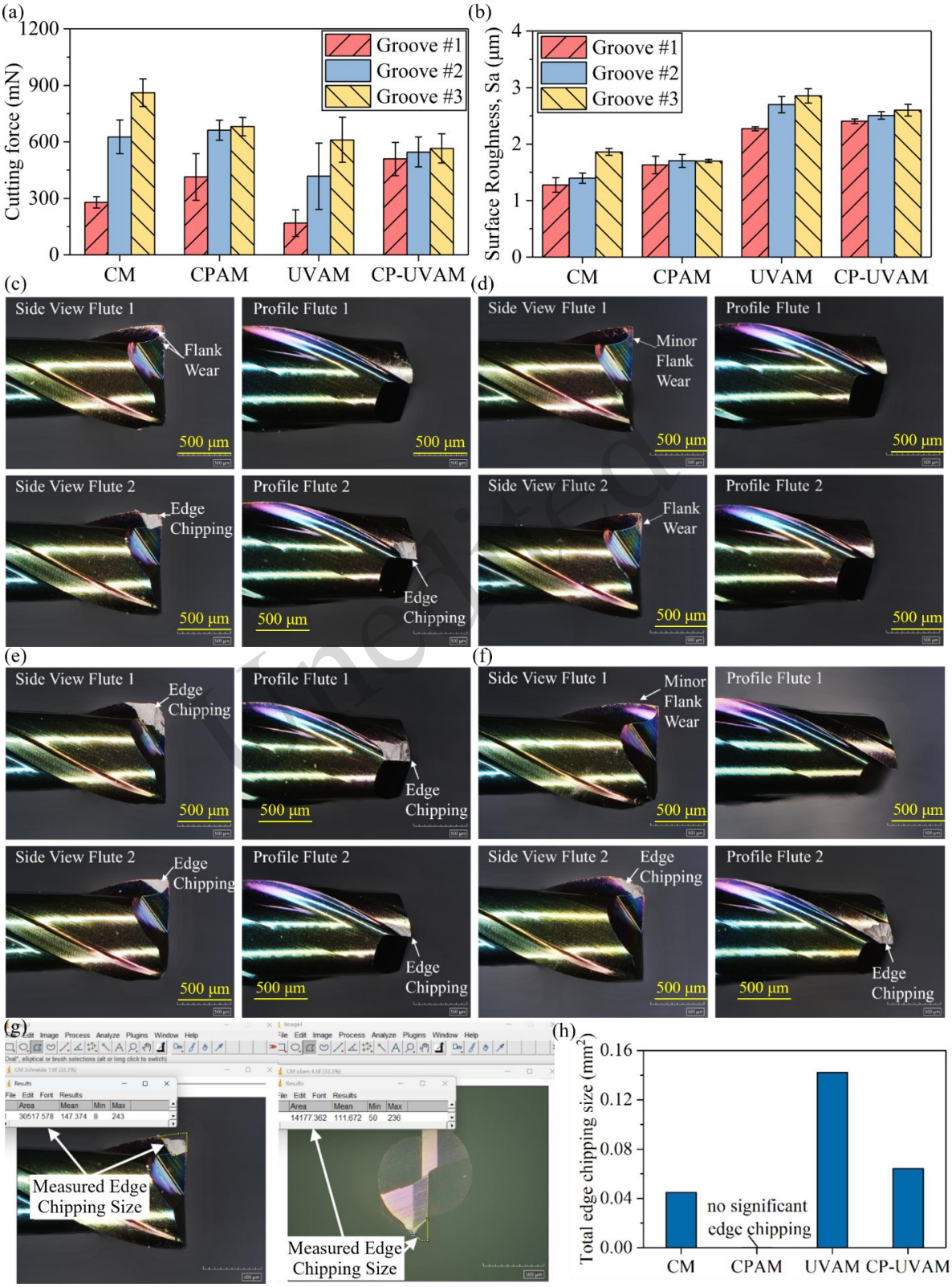

Fig. 4 Micro-milling performance of BMGs under various milling strategies. (a) Average cutting force of grooves machined by different milling methods; (b) Surface roughness of grooves machined by different milling methods; (c) Tool wear of CM; (d) Tool wear of CPAM; (e) Tool wear of UVAM; (f) Tool wear of CP-UVAM; (g) Exemplary measured edge chipping size of a flute from side and end views using ImageJ; (h) Total tool edge chipping size by different milling

methods

3.3.3 Tool wear

As seen in **Fig. 4**c, the two primary defects observed on the cutting tool are flank wear and edge chipping. The flank wear is particularly visible from the side view of Flute 1; it is characterized by the abrasion of the diamond-like coating of the milling tool. This wear can lead to increased friction and heat generation during the milling process, which in turn increases the wear rate of the tool. Moreover, the removal of the coating exposes the underlying material to further wear and potential failure, compromising the tool's cutting efficiency and precision. Edge chipping, on the other hand, occurred primarily at Flute 2 and is visible from the profile, side, and top views. The edge chipping size was quantified using *ImageJ* software (**Fig. 4**g). After setting a scale, the software measured the area of edge chipping (when present) from both the side and top views for each cutting edge. The total edge chipping area per tool was calculated by summing the measurements from both views and both cutting edges, providing a comparative metric for tool wear assessment across milling experiments. The area of the chipped edge was 0.0447 mm^2, which aligns with the typical tool failure modes reported in conventional micro-milling of hard, brittle BMGs, where high intermittent stresses often lead to catastrophic edge fractures rather than gradual flank wear. This is likely the reason for the drastic deterioration in the exerted cutting forces and resulting surface quality, especially in groove #3 for the CM approach. The presence of edge chipping can significantly affect the surface finish of the milled grooves. This type of wear is often caused by the high mechanical stresses and impact forces encountered during milling of hard materials like BMGs.

Optical microscopy images of the milling tool using CPAM are displayed in **Fig. 4**d. Similar to the findings regarding cutting forces and surface quality in the CPAM approach, the tool wear in CPAM is minimal compared to CM. The primary negative consequence regarding tool wear in CM, edge chipping, did not occur in CPAM. Furthermore, the flank wear on the flutes is significantly less pronounced than in CM. Minor flank wear is visible from the side view of Flute 1, which is not noticeable from the profile and top views. The flank wear on Flute 2 is slightly more pronounced – as seen in the side view – but it is still minimal compared to CM. This dramatic suppression of edge chipping strongly supports the mechanism proposed by Lv et al. (2022), and is also evidenced by our nanoindentation results: the plasma-induced increase in free volume and enhanced plastic deformability at the BMG surface allow for stress relaxation and more stable material removal, thereby reducing the high-impact, brittle fracture events that cause tool edge failure. The absence of chipping in CPAM is a more significant benefit than the general flank wear reduction reported in plasma-assisted machining of crystalline alloys (Liu et al., 2021), thus highlighting the unique value of CP for mitigating the brittleness of BMGs. In summary, the observations of tool wear are in line with the investigations of cutting force and surface quality, which clearly showed consistent material removal. This consistency is reflected in the minimal tool wear observed in CPAM.

The morphology of the used milling tool from UVAM is displayed in **Fig. 4**e. UVAM resulted in severe tool wear in the form of extensive edge chipping on both flutes. The edge chipping on Flute 1 is particularly drastic. The chipped area is more than twice as large, with 0.074 mm^2 compared to 0.031 mm^2 in CM, as observed from the side view. Additionally, the depth of the chipping – visible in the top view – is almost three times larger, measuring 0.041 mm^2 compared to 0.014 mm^2 in CM. Furthermore, edge chipping occurred on both flutes. Flute 2, although not as severely affected as Flute 1, still shows a total chipped area of 0.027 mm^2 compared to 0.0447 mm^2 in CM. This severe and accelerated edge chipping (a 217.70% increase in total area) provides a critical, physically observable explanation for the force instability and surface degradation reported in Section 3.3.2. It also corroborates the concern raised by Chen et al. (2022) regarding potential tool damage in UVAM of BMGs. The high-frequency impact in UVAM appears to exacerbate, rather than alleviate, the brittle fracture-induced tool failure mechanism in BMGs, a finding that contrasts with UVAM's often-reported

tool life benefits in machining more ductile materials. This underscores the material-specific challenges and risks of applying UVAM to BMGs without compensatory strategies. Furthermore, this severe tool wear is likely the reason for the drastic deterioration in surface quality observed throughout the milling process.

Fig. 4f shows the morphology of the used milling tool of CP-UVAM. It can be seen that the cold plasma pre-treatment of the surface had a positive effect on tool wear. While Flute 2 is affected by some prominent edge chipping, Flute 1 only shows minor flank wear. Quantitatively, the size of the chipped edge on Flute 2 is almost half that of UVAM alone, with a total edge chipping size of 0.064 mm^2 compared to the severe edge chipping of 0.115 mm^2 on Flute 2 in UVAM. Most importantly, the synergistic CP-UVAM approach reduced the total edge chipping by 43.97% compared to standalone UVAM. This indicates that the plasma pretreatment effectively mitigated the primary drawback of UVAM. The mechanism behind this is twofold: first, the plasma-softened surface layer reduces the instantaneous impact stress on the tool edge during each vibration cycle; second, the improved surface wettability ensures better lubricant access to the cutting zone, reducing friction and heat. This synergistic protection is a novel finding, demonstrating that CP pretreatment can expand the viable window of parameters for UVAM of BMGs by making the tool less susceptible to vibration-induced fracture. Nevertheless, the total edge chipping size of the tool in CP-UVAM, at 0.064 mm^2, is still higher than the 0.0447 mm^2 in CM, and of course than the complete absence of edge chipping in CPAM. This explains why, despite the low cutting forces applied, there was still a slightly non-uniform texture on the BMG surface.

The total edge chipping sizes of the tool are graphically depicted in **Fig. 4**h. CM exhibited significant tool wear, primarily in the form of flank wear and edge chipping. The edge chipping on Flute 2 – with an area of 0.0447 mm^2 – likely contributed to the significantly deteriorated surface quality, especially in groove #3. In contrast, CPAM demonstrated minimal tool wear compared to CM. The detrimental edge chipping observed in CM did not occur in CPAM, and the flank wear on the flutes was much less pronounced. This observation of minimal tool wear aligns with the consistent material removal and stable surface quality noted in CPAM, supporting the notion that cold plasma treatment enhances tool longevity and performance.

UVAM was accompanied by severe tool wear, in particular extensive edge chipping on both flutes. The chipped area on Flute 1 was more than twice as large as in CM, and the depth of the chipping was almost three times larger; there was a total edge chipping size of 0.142 mm^2, which is an increase of 217.70 % compared to CM. This severe tool wear likely caused the drastic deterioration in surface quality observed in the milling process from groove #2 onwards.

CP-UVAM showed more promising results compared to UVAM alone. The pre-treatment of BMG with cold plasma reduced the severity of edge chipping, particularly by preventing chipping on one flute and reducing the edge chipping size on the other, where the chipped edge size was only about half that of UVAM alone. However, the total edge chipping size in CP-UVAM was still 43.97% higher than in CM with 0.064 mm^2, indicating that while cold plasma treatment mitigated some wear effects, it could not entirely prevent edge chipping. This analysis of tool wear demonstrates the complementary roles of each technique: CPAM excels at preventing tool damage by conditioning the material, UVAM markedly reduces forces but at a high cost to tool integrity, and CP-UVAM successfully integrates both of these benefits, achieving significant force reduction while maintaining tool condition far better than UVAM alone. This optimal trade-off and synergy are central to the practical viability of the proposed strategy.

4 Conclusions

We demonstrated that cold plasma treatment significantly enhances micro-milling of BMGs by transforming their surfaces from hydrophobic to super hydrophilic, improving coolant penetration and reducing shear band initiation resistance. This result was confirmed by nano-indentation and scratching tests. The increased plastic deformability resulting from cold plasma alone enabled smoother material removal; accordingly, this approach achieved the best surface quality and minimal tool wear, highlighting its standalone efficacy. Meanwhile, ultrasonic

vibration reduced cutting forces through high-frequency oscillations, but also caused severe tool edge chipping, degrading surface quality over time. However, the combined CP-UVAM approach synergistically mitigated these drawbacks: cold plasma's lubrication and deformability improvements counteracted the UV-induced tool wear, while ultrasonic vibration's force reduction complemented cold plasma's material softening, resulting in stable cutting forces, minimal edge chipping, and superior surface consistency. These findings underscore cold plasma's pivotal role—both independently and in hybrid processes—in overcoming the challenges of machining brittle amorphous alloys. Therefore this hybrid approach offers a promising pathway for advanced BMG machining strategies.

Acknowledgments

The authors gratefully acknowledge the financial support for this research provided by the National Natural Science Foundation of China (Grant No. 52475470, 124115301, 52505495), Huaneng Group Science and Technology Research Project (No: HNKJ22-H105), the Postdoctoral Fellowship Program of CPSF under Grant Number GZC20240816.

Author contributions

Jianjian Wang designed the research. Emek Babuskin KOCYIGIT and Qilin Li processed the corresponding data. Qilin Li wrote the first draft of the manuscript. Long YE and Nan YU contributed to data visualization and graphical illustration. Pingfa FENG helped to organize the manuscript. Jianjian Wang revised and edited the final version.

Conflict of interest

Qilin Li, Emek Babuskin KOCYIGIT, Long YE, Nan YU, Pingfa FENG and Jianjian Wang declare that they have no conflict of interest.

References

Chen Z, Feng P, Wang J, et al., 2022. Understanding the abnormal effects of ultrasonic vibration on tool wear and surface generation in Zr-based bulk metallic glass cutting. *CIRP Journal of Manufacturing Science and Technology*, 2022, 39:1–17. https://doi.org/10.1016/j.cirpj.2022.07.004.

Zhang L, Huang H, 2019. Micro machining of bulk metallic glasses: a review. *The International Journal of Advanced Manufacturing Technology*, 100(1):637–661. https://doi.org/10.1007/s00170-018-2726-y.

Xie B, Kumar M N, Yan D P, et al., 2017. Material behavior in micro milling of zirconium based bulk metallic glass. TMS 2017 146th Annual Meeting & Exhibition Supplemental Proceedings. Springer: 363–373. https://doi.org/10.1007/978-3-319-51493-2_34

Wang T, Wu X, Zhang G, et al., 2020. Experimental study on machinability of Zr-based bulk metallic glass during micro milling. *Micromachines*, 11(1):86. https://doi.org/10.3390/mi11010086.

Ray D, Puri A B, Nagahanumaiah., 2019. Investigation on cutting forces and surface finish in mechanical micro milling of Zr-based bulk metallic glass. *Journal of Advanced Manufacturing Systems*, 18(01):113–132. https://doi.org/10.1142/S0219686719500069.

Wang T, Wu X, Zhang G, et al., 2020. Study on surface roughness and top burr of micro-milled Zr-based bulk metallic glass in shear dominant zone. *The International Journal of Advanced Manufacturing Technology*, 107:4287–4299. https://doi.org/10.1007/s00170-020-05325-7.

Gao G, Sun Z, Pan X, et al., 2023. Study of longitudinal-torsional ultrasonic-assisted vibration on micro-hole drilling Zr-based metallic glass. *The International Journal of Advanced Manufacturing Technology*, 131: 2893–2907. https://doi.org/10.1007/s00170-023-12649-7.

Shan S, Feng P, Zha H, et al., 2020. Building of longitudinal ultrasonic assisted turning system and its cutting simulation study on bulk metallic glass. *Materials*, 13(14):3131. https://doi.org/10.3390/ma13143131.

Liu J, Song J, Chen Y, et al., 2021. Atmospheric pressure cold plasma jet–assisted micro-milling TC4 titanium alloy. *The International Journal of Advanced Manufacturing Technology*, 112(7):2201–2209. https://doi.org/10.1007/s00170-020-06488-z.

Mustafa G, Liu J, Zhang F, et al., 2019. Atmospheric pressure plasma jet assisted micro-milling of Inconel 718. *The International Journal of Advanced Manufacturing Technology*, 103:4681–4687. https://doi.org/10.1007/s00170-019-03931-8.

Wang Z, Li Y, Wang S, et al., 2024. Feasibility and mechanism of atmospheric pressure cold plasma jet (APCPJ) assisted micro-milling of bulk metallic glasses (BMGs). *Ceramics International*, 50(7): 1094-11105 https://doi.org/10.1016/j.ceramint.2024.01.011.

Li H, Yang J, Zhang C, et al., 2025. Different non-traditional energy fields assisted milling of SiCf/SiC composites: Investigation on tool wear mechanisms and effects on machined surface quality. *Wear*, 571:205844. https://doi.org/10.1016/j.wear.2025.205844.

Lv J W, Wei C, Shi Z L, et al., 2022. The size-dependence of compressive mechanical properties and serrated-flow behavior of Ti-based bulk metallic glass. *Materials Science and Engineering A*, 857:143968. https://doi.org/10.1016/j.msea.2022.143968.

Bakkal M, Liu C T, Watkins T R, et al., 2004. Oxidation and crystallization of Zr-based bulk metallic glass due to machining. *Intermetallics*, 12(2):195–204. https://doi.org/10.1016/j.intermet.2003.09.017.

Yamamura K, Takiguchi T, Ueda M, et al., 2010. High-Integrity Finishing of 4H-SiC (0001) by Plasma-Assisted Polishing. *Advanced Materials Research*, 126–128:423–8. https://doi.org/10.4028/www.scientific.net/AMR.126-128.423.

Liu X, Wang B, Li Y, et al., 2023. Improving machinability of single-crystal silicon by cold plasma jet. *Journal of Manufacturing Processes*, 99:581–91. https://doi.org/10.1016/j.jmapro.2023.05.071.

Schuh C A, Nieh T G, 2003. A nanoindentation study of serrated flow in bulk metallic glasses, *Acta Materialia*, 51(1):87–99. https://doi.org/10.1016/S1359-6454(02)00303-8.

Puthucode A, Banerjee R, Vadlakonda S, et al., 2008. Incipient Plasticity and Shear Band Formation in Bulk Metallic Glass Studied Using Indentation. *Metallurgical and Materials Transactions A*, 39(7):1552–1559. https://doi.org/10.1007/s11661-007-9338-8.

中文概要

题　目：低温等离子体与超声振动协同增效的金属玻璃微铣削研究

作　者：李麒麟[1,2]，Emek Babuskin KOCYIGIT[1,2]，叶龙[3]，于楠[3]，冯平法[1,2]，王健健[1,2]

机　构：[1]清华大学，机械工程系，先进装备摩擦学国家重点实验室，中国北京，100084；[2]清华大学，机械工程系，北京精密/超精密制造装备与控制重点实验室，中国北京，100084；[3]爱丁堡大学，工程学院材料与过程研究所，英国苏格兰爱丁堡，EH9 3FB

目　的：块状金属玻璃具有优异的力学性能，但因其高硬度和高脆性导致可加工性差，传统微铣削易造成刀具快速磨损和表面缺陷。本文旨在探究冷等离子体预处理与超声振动辅助微铣削的协同作用，开发一种新型复合加工策略，以提升金属玻璃的微铣削质量与效率。

创新点：1. 提出并研究了金属玻璃低温等离子体预处理与超声振动辅助微铣削相结合的加工方法；2. 明确了低温等离子体预处理与超声振动辅助微铣削的协同效应，在实现切削力降低的同时，有效抑制了刀具磨损。

方　法：1. 通过接触角测量、纳米压痕与纳米划痕实验，量化等离子体处理对金属玻璃表面润湿性、弹性模量与塑性变形行为的影响；2. 采用四种工艺方法（传统铣削、低温等离子体辅助铣削、超声振动辅助铣削及两者结合的方法）进行微铣削对比试验；3. 使用测力仪测量切削力，激光共聚焦显微镜分析表面粗糙度，超景深显微镜观察刀具磨损与刃口崩缺，系统评价各方法的加工性能。

结　论：1. 低温等离子体预处理能显著地提升金属玻璃的可加工性，实现最佳表面质量与最小刀具磨损；2. 超声振动辅助铣削虽可降低平均切削力，但会引发严重的刀具刃口崩缺，导致加工过程不稳定与表面质量下降；3. 所提出的低温等离子体预处理与超声振动辅助微铣削复合工艺发挥了协同优势：在保留超声振动降低切削力效果的同时，大幅减轻了超声振动引起的刀具损伤，获得了更稳定、一致的表面质量。

关键词：金属玻璃；微铣削；低温等离子体；超声振动；